Research Article | Vol. 27, No. 26 / 23 December 2019 / Optics Express 37494

Optics EXPRESS

Non-*PT*-symmetric two-layer cylindrical waveguide for exceptional-point-enhanced optical devices

YIN HUANG,[1,5] YUECHENG SHEN,[2,6] AND GEORGIOS VERONIS[3,4]

[1]*Department of Optoelectrics Information Science and Engineering, School of Physics and Electronics, Central South University, Changsha, Hunan 410012, China*
[2]*State Key Laboratory of Optoelectronic Materials and Technologies, School of Electronics and Information Technology, Sun Yat-Sen University, Guangzhou, Guangdong 510275, China*
[3]*School of Electrical Engineering and Computer Science, Louisiana State University, Baton Rouge, LA 70803, USA*
[4]*Center for Computation and Technology, Louisiana State University, Baton Rouge, LA 70803, USA*
[5]*yhuan15@csu.edu.cn*
[6]*shenyuecheng@mail.sysu.edu.cn*

Abstract: We investigate the exceptional points in a two-layer cylindrical waveguide structure consisting of absorbing and non-absorbing dielectrics. We show that, by tuning the core to total radius ratio and the refractive index of the core layer in such a structure, the complex effective indices of two waveguide modes can coalesce so that an exceptional point is formed. We show that the sensitivity of the effective index of the waveguide mode to variations of the refractive index of the material filling the shell layer is enhanced at the exceptional point. In addition, we show that larger sensitivity enhancement is obtained for smaller perturbations. Our results could potentially contribute to the development of a new generation of chip-scale exceptional-point-enhanced optical waveguide devices for modulation, switching, and sensing.

1. Introduction

Exceptional points (EPs), associated with the coalescence of both the eigenvalues and the corresponding eigenstates of open quantum systems described by non-Hermitian Hamiltonians, have attracted a lot of attention in recent years [1–5]. EPs have been investigated in ultrasonic cavities [6], mechanics [7], electronic circuits [8], and molecular systems [9]. EPs in non-Hermitian optical systems can lead to numerous interesting phenomena such as power oscillation [10,11], optical isolation [12], unidirectional light reflection [13–15], perfect absorption [16–18], enhanced sensing [19–22], directional lasing [23,24], neuromorphic photonics [25], slow light [26], topological waveguiding [27], and others [28–35]. In optical waveguide systems, EPs have been observed in coupled waveguide structures with parity-time (*PT*) symmetry. In such structures one of two parallel waveguides experiences gain, while the other one experiences an equal amount of loss [11,36]. Recently, Alaeian *et al*. reported observing EPs in a single three-layer cylindrical coaxial waveguide consisting of a dielectric layer sandwiched between two silver layers after introducing balanced gain and loss azimuthally within the dielectric layer [37]. However, these *PT*-symmetric optical systems are hard to implement in practice, because the required periodic modulation of the refractive index profile necessitates careful tuning of both the real and imaginary parts of the refractive indices of the constituent materials. EPs have also been observed in non-*PT*-symmetric structures with unbalanced gain and loss [29,38–41]. In particular, Doppler *et al*. and Ke *et al*. showed that EPs exist in coupled waveguide structures without gain media [29,38]. This is due to the fact that EPs exist in a larger family of non-Hermitian Hamiltonians, since *PT*-symmetry is not a necessary condition for the existence of EPs [40,41].

#380384 https://doi.org/10.1364/OE.27.037494
Journal © 2019 Received 15 Oct 2019; revised 2 Dec 2019; accepted 3 Dec 2019; published 11 Dec 2019

Optics EXPRESS

Designing single non-*PT*-symmetric waveguides to exhibit EPs could be essential for developing compact and easy-to-implement exceptional-point-enhanced optical devices.

In this paper, we investigate the EPs in a two-layer cylindrical waveguide structure consisting of absorbing and non-absorbing dielectrics. The effective indices of the propagating waveguide modes are the eigenvalues of the non-Hermitian system, and the corresponding propagating waveguide modes are the system eigenfunctions. We show that, by tuning the core to total radius ratio and the refractive index of the core layer, the complex effective indices of two waveguide modes can coalesce so that an EP is formed. We investigate the properties of the realized EP of the structure, as well as the associated physical effects of level repulsion and crossing. We show that the sensitivity of the effective index of the waveguide mode to variations of the refractive index of the material filling the shell layer is enhanced at the EP. In addition, we show that larger sensitivity enhancement is obtained for smaller perturbations. We also find that, as the loss in the shell layer increases, the sensitivity increases. Our results could potentially contribute to the development of a new generation of chip-scale exceptional-point-enhanced optical waveguide devices for modulation, switching, and sensing.

The remainder of the paper is organized as follows. In Section 2, we review the transfer matrix method which can account for the behavior of the proposed two-layer cylindrical waveguide structure. In Subsection 3.1 we use this theory to show that the two-layer cylindrical waveguide structure when properly designed exhibits an EP. The realized EP of the structure and its topological properties are then investigated in Subsection 3.2. In Subsection 3.3 we investigate the sensitivity of the effective index of the waveguide mode of the structure to variations of the refractive index of the material filling the shell layer at the EP. Finally, our conclusions are summarized in Section 4.

2. Theory

Our proposed two-layer cylindrical waveguide structure consists of absorbing and non-absorbing dielectrics (Fig. 1). The general solution for the modal fields of a circularly symmetric cylindrical waveguide can be written in the following form [42]

$$\mathbf{F}(r,\phi,z) = \mathbf{f}(r)e^{j(m\phi+\beta z)}, \tag{1}$$

where $\mathbf{f} = (\mathbf{e}, \mathbf{h})$ is a six-component electromagnetic field vector that only depends on r, β is the complex wavevector of the waveguide mode, and m is the azimuthal mode number. By expanding the fields in terms of cylindrical wave functions [42–45], the electromagnetic fields in each region can be expressed as follows: The fields in the core layer ($r<a_1$) with refractive index n_1 are given by

$$\begin{bmatrix} e_\phi \\ e_z \\ h_\phi \\ h_z \end{bmatrix} = M_1 \begin{bmatrix} A_{e1} \\ B_{e1} \\ A_{h1} \\ B_{h1} \end{bmatrix}, \tag{2}$$

where

$$M_1 = \begin{bmatrix} \frac{-m\beta J_m(U_1 r)}{{U_1}^2 r} & \frac{-m\beta J_m(U_1 r)}{{U_1}^2 r} & \frac{-j\omega\mu_0 J_m'(U_1 r)}{U_1} & \frac{-j\omega\mu_0 N_m'(U_1 r)}{U_1} \\ J_m(U_1 r) & N_m(U_1 r) & 0 & 0 \\ \frac{j\omega\epsilon_1 J_m'(U_1 r)}{U_1} & \frac{j\omega\epsilon_1 N_m'(U_1 r)}{U_1} & \frac{-m\beta J_m(U_1 r)}{{U_1}^2 r} & \frac{-m\beta J_m(U_1 r)}{{U_1}^2 r} \\ 0 & 0 & J_m(U_1 r) & N_m(U_1 r) \end{bmatrix}, \tag{3}$$

$U_1^2 = n_1^2 k_0^2 - \beta^2$, k_0 is the wavenumber in free space, μ_0 is the magnetic permeability of free space, and $\epsilon_1 = n_1^2$. J_m and N_m are the m-th order Bessel functions of the first and second

Optics EXPRESS

kind, respectively. The complex effective index n_{eff} and wavevector β of the waveguide mode are related through $\beta = k_0 n_{\text{eff}}$. A_{e1}, B_{e1}, A_{h1}, and B_{h1} are field coefficients [42]. Note that $B_{e1} = B_{h1} = 0$, which is due to the fact that the field components have to converge at the origin of coordinates. Similarly, the fields in the shell ($a_1 < r < a_2$) with refractive index n_2 (Fig. 1) can be written as

$$\begin{bmatrix} e_\phi \\ e_z \\ h_\phi \\ h_z \end{bmatrix} = M_2 \begin{bmatrix} A_{e2} \\ B_{e2} \\ A_{h2} \\ B_{h2} \end{bmatrix}, \tag{4}$$

where

$$M_2 = \begin{bmatrix} \frac{-m\beta J_m(U_2 r)}{{U_2}^2 r} & \frac{-m\beta J_m(U_2 r)}{{U_2}^2 r} & \frac{-j\omega\mu_0 J'_m(U_2 r)}{U_2} & \frac{-j\omega\mu_0 N'_m(U_2 r)}{U_2} \\ J_m(U_2 r) & N_m(U_2 r) & 0 & 0 \\ \frac{j\omega\epsilon_2 J'_m(U_2 r)}{U_2} & \frac{j\omega\epsilon_2 N'_m(U_2 r)}{U_2} & \frac{-m\beta J_m(U_2 r)}{{U_2}^2 r} & \frac{-m\beta J_m(U_2 r)}{{U_2}^2 r} \\ 0 & 0 & J_m(U_2 r) & N_m(U_2 r) \end{bmatrix}, \tag{5}$$

$U_2^2 = n_2^2 k_0^2 - \beta^2$, and $\epsilon_2 = n_2^2$. A_{e2}, B_{e2}, A_{h2}, and B_{h2} are field coefficients. The fields outside the cylindrical waveguide structure ($r > a_2$) are expressed as

$$\begin{bmatrix} e_\phi \\ e_z \\ h_\phi \\ h_z \end{bmatrix} = M_3 \begin{bmatrix} A_{e3} \\ B_{e3} \\ A_{h3} \\ B_{h3} \end{bmatrix}, \tag{6}$$

where

$$M_3 = \begin{bmatrix} \frac{m\beta I_m(Wr)}{W^2 r} & \frac{m\beta K_m(Wr)}{W^2 r} & \frac{j\omega\mu_0 I'_m(Wr)}{U_1} & \frac{j\omega\mu_0 K'_m(Wr)}{W} \\ I_m(Wr) & K_m(Wr) & 0 & 0 \\ \frac{-j\omega\epsilon_3 I'_m(Wr)}{W} & \frac{-j\omega\epsilon_3 K'_m(Wr)}{W} & \frac{m\beta I_m(Wr)}{W^2 r} & \frac{m\beta K_m(Wr)}{W^2 r} \\ 0 & 0 & I_m(Wr) & K_m(Wr) \end{bmatrix}, \tag{7}$$

$W^2 = \beta^2 - n_3^2 k_0^2$, and $n_3 = 1$ is the refractive index of free space. I_m and K_m are the m-th order modified Bessel functions of the first and second kind, respectively. A_{e3}, B_{e3}, A_{h3}, and B_{h3} are field coefficients. Note that $A_{e3} = A_{h3} = 0$, which is due to the fact that the electromagnetic fields of the waveguide mode have to fulfill an outgoing wave boundary condition at infinity [42]. By enforcing the boundary conditions for the electromagnetic field components at each interface $r = a_i$, $i = 1, 2$ and using the transfer matrix method [42,46], we derive the following equation which relates the field coefficients in the core and air regions

$$\begin{bmatrix} 0 \\ B_{e3} \\ 0 \\ B_{h3} \end{bmatrix} = M_{23} M_{12} \begin{bmatrix} A_{e1} \\ 0 \\ A_{h1} \\ 0 \end{bmatrix} = \begin{bmatrix} m_{1,1} & m_{1,2} & m_{1,3} & m_{1,4} \\ m_{2,1} & m_{2,2} & m_{2,3} & m_{2,4} \\ m_{3,1} & m_{3,2} & m_{3,3} & m_{3,4} \\ m_{4,1} & m_{4,2} & m_{4,3} & m_{4,4} \end{bmatrix} \begin{bmatrix} A_{e1} \\ 0 \\ A_{h1} \\ 0 \end{bmatrix}, \tag{8}$$

Optics EXPRESS

where $M_{12} = M_2^{-1}\big|_{r=a_1} M_1\big|_{r=a_1}$, and $M_{23} = M_3^{-1}\big|_{r=a_2} M_2\big|_{r=a_2}$. The above equation can be further reduced to

$$\begin{bmatrix} m_{1,1} & m_{1,3} \\ m_{3,1} & m_{3,3} \end{bmatrix} \begin{bmatrix} A_{e1} \\ A_{h1} \end{bmatrix} = 0. \tag{9}$$

We can therefore obtain the effective index n_{eff} of the propagating modes by solving the following nonlinear equation

$$\begin{vmatrix} m_{1,1} & m_{1,3} \\ m_{3,1} & m_{3,3} \end{vmatrix} = m_{1,1}(n_{\text{eff}})m_{3,3}(n_{\text{eff}}) - m_{1,3}(n_{\text{eff}})m_{3,1}(n_{\text{eff}}) = 0. \tag{10}$$

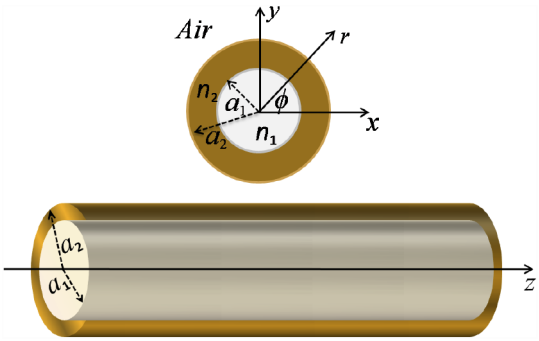

Fig. 1. Schematics of a two-layer core-shell cylindrical waveguide structure.

3. Results

We optimize the core to total radius ratio $\chi = \frac{a_1}{a_2}$ (Fig. 1), and the refractive index of the core layer n_1, to obtain a core-shell cylindrical waveguide structure as in Fig. 1 which exhibits an EP. Equation (10) is numerically solved using Newton's method [47] to calculate the effective index n_{eff} of the propagating modes. Since various classes of materials such as semiconductors and oxides have high refractive indices up to 3.4 [48], the refractive index of the core layer in our structure n_1 is optimized within the range from 2 to 3.4. The shell layer is filled with an active material with refractive index $n_2 = 2.02 + j\kappa$, corresponding to silicon dioxide doped with CdSe quantum dots [49–51]. The imaginary part κ of the refractive index can be modified with an external control beam [49,51]. In addition, we choose $k_0 a_2 = 10$, so that the proposed waveguide structure supports multiple propagating modes.

3.1. Location of exceptional points

Here we choose $\kappa = 0.05$ for the imaginary part of the refractive index n_2 of the material filling the shell layer (Fig. 1), which is within the range of experimentally achievable values [50,51]. By solving Eq. (10) using Newton's method, we find that an EP emerges for $n_1 = 2.875$, $\chi = \frac{a_1}{a_2} = 0.514$, and azimuthal mode number of $m = 6$. At this EP, the real and imaginary parts of the effective indices of two waveguide modes coalesce at $n_{\text{eff}} = 1.497 + j0.046$.

Similar to PT-symmetric quantum systems, PT-symmetric optical systems possess two different phases [11,21]. The first phase is the PT-unbroken phase with real eigenvalues. The second phase is the PT-broken phase characterized by complex conjugate eigenvalues with equal real parts but opposite imaginary parts. The transition between the two phases takes place at the EP where the two eigenvalues coalesce. Figure 2(a) shows a particular curve that we found in

Optics EXPRESS

the $\chi - n_1$ design parameter space, where either the real parts or the imaginary parts of the effective indices of the two waveguide modes coincide. We parameterize this parameter curve by $\Gamma = -sgn(\Delta\chi)\sqrt{(\Delta\chi)^2 + (\Delta n_1)^2}$, where $\Delta\chi = (a_1 - a_{1,\mathrm{EP}})/a_2 = \chi - \chi_{\mathrm{EP}}$, $\Delta n_1 = n_1 - n_{1,\mathrm{EP}}$, and *sgn* is the sign function. In Figs. 2(b) and 2(c) we show the evolution of the real and imaginary parts, respectively, of the eigenvalues n_{eff} of the two waveguide modes along the particular curve parametrized by Γ in the $\chi - n_1$ design parameter space. We observe that for $\Gamma>0$, the two eigenvalues have equal real parts but different imaginary parts, which is analogous to the *PT*-symmetric broken regime. When Γ decreases to zero, the two eigenvalues coalesce and the EP is formed. For $\Gamma<0$, the real parts of the eigenvalues bifurcate and their imaginary parts merge, which actually resembles the *PT*-symmetric unbroken regime. Note that the imaginary part of the eigenvalues for $\Gamma<0$ is non-zero, and the imaginary parts of the eigenvalues for $\Gamma>0$ are not conjugate [Fig. 2(c)]. This is due to the fact that our proposed waveguide structure (Fig. 1) is a non-Hermitian optical system without gain, which is different from conventional *PT*-symmetric non-Hermitian optical systems with balanced gain and loss [11,21].

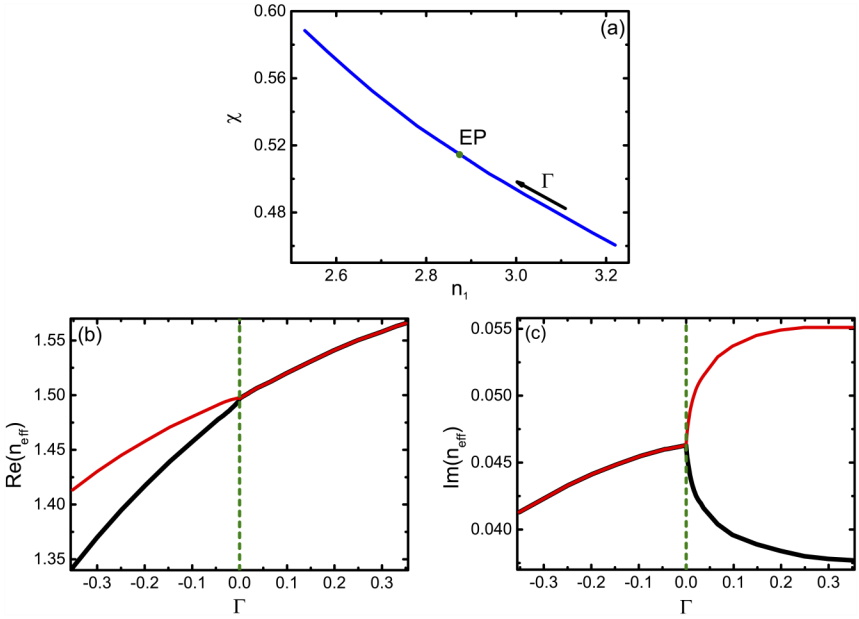

Fig. 2. (a) A curve in the $\chi - n_1$ design parameter space parameterized by $\Gamma = -sgn(\Delta\chi)\sqrt{(\Delta\chi)^2 + (\Delta n_1)^2}$ (blue line), where either the real parts or the imaginary parts of the effective indices of the two waveguide modes coincide. The exceptional point is located at $(\chi, n_1) = (0.514, 2.875)$ (green dot). Results are shown for $n_2 = 2.02 + j0.05$, $k_0 a_2 = 10$, and $m = 6$. (b) and (c) Real and imaginary parts of the effective indices of the two waveguide modes (black and red lines) along the curve parametrized by Γ [Fig. 2(a)]. All other parameters are as in Fig. 2(a). The green vertical dashed lines indicate the location of the exceptional point ($\Gamma = 0$).

To understand the underlying formation mechanisms of the EPs in our proposed two-layer cylindrical waveguide system, the transverse field intensity distributions $|e_\phi|^2$ along the curve Γ [Fig. 2(a)] are shown in Fig. 3. More specifically, Figs. 3(a) and 3(b) show the field intensity distributions $|e_\phi|^2$ for the waveguide modes with effective indices $n_{\mathrm{eff}} = 1.5658 + j0.0373$ and $n_{\mathrm{eff}} = 1.5658 + j0.0552$, respectively, for $\Gamma = 0.35$ (Fig. 2). We observe that one eigenmode is mostly localized in the core region [Fig. 3(a)] and will therefore be referred to as the core mode, while the other eigenmode is mostly localized in the shell layer [Fig. 3(b)] and will therefore

Optics EXPRESS

be referred to as the shell mode. Figure 3(c) shows the field intensity distribution $|e_\phi|^2$ for the degenerate mode with effective index $n_{\text{eff}} = 1.497 + j0.046$ at the EP ($\Gamma = 0$ in Fig. 2). We observe that for the waveguide mode at the EP the field intensity is strong in both the core and shell regions. Figures 3(d) and 3(e) show the field intensity distributions $|e_\phi|^2$ for the waveguide modes with effective indices $n_{\text{eff}} = 1.3423 + j0.0413$ and $n_{\text{eff}} = 1.4133 + j0.0413$, respectively, for $\Gamma = -0.35$ (Fig. 2). We observe that hybrid modes are formed due to the strong intermode interaction between the two eigenmodes as the core to total radius ratio χ further increases along the curve parametrized by Γ [Fig. 2(a)]. The EP is therefore the point of transition between the strong intermode interaction phase and the weak intermode interaction phase. Similar kinds of EPs have been observed in two-dimensional concentric circular cavity structures [6,52].

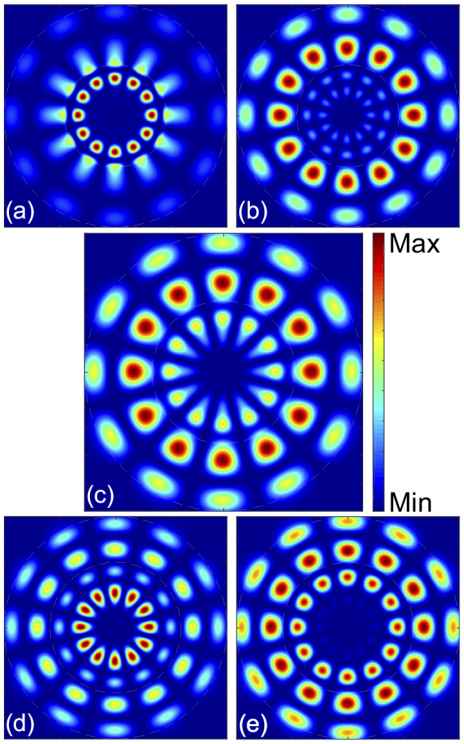

Fig. 3. (a) and (b) Field intensity distributions $|e_\phi|^2$ of the waveguide modes along the curve parametrized by Γ [Fig. 2(a)] for the structure of Fig. 1 for $\Gamma = 0.35$ ($\chi = 0.461, n_1 = 3.220$). All other parameters are as in Fig. 2(a). (c) Field intensity distribution $|e_\phi|^2$ of the waveguide modes along the curve parametrized by Γ [Fig. 2(a)] for the structure of Fig. 1 at the exceptional point ($\Gamma = 0$ corresponding to $\chi = 0.514, n_1 = 2.875$). All other parameters are as in Fig. 2(a). (d) and (e) Field intensity distributions $|e_\phi|^2$ of the waveguide modes along the curve parametrized by Γ [Fig. 2(a)] for the structure of Fig. 1 for $\Gamma = -0.35$ ($\chi = 0.588, n_1 = 3.530$). All other parameters are as in Fig. 2(a). The dashed lines indicate the interfaces $r = a_i$, $i = 1, 2$ between different regions of the structure (Fig. 1).

In addition, the occurrence of EPs in our proposed two-layer waveguide structure (Fig. 1), when the real and imaginary parts of the eigenvalues n_{eff} of the two waveguide modes evolve along the curve parametrized by Γ [Fig. 2(a)], can be illustrated with a two-level model. The

Optics EXPRESS

corresponding non-Hermitian Hamiltonian is given by [5]

$$H = \begin{bmatrix} n_{r,\text{eff}} + jn_{i,\text{eff}} & \gamma \\ \gamma & \widetilde{n}_{r,\text{eff}} + j\widetilde{n}_{i,\text{eff}} \end{bmatrix}, \tag{11}$$

where the off-diagonal elements, which are equal to γ, are associated with the coupling strength between the propagating waveguide modes, while the diagonal elements correspond to the complex refractive indices $n_{r,\text{eff}} + jn_{i,\text{eff}}$ and $\widetilde{n}_{r,\text{eff}} + j\widetilde{n}_{i,\text{eff}}$ of the uncoupled propagating waveguide modes. Here, the two uncoupled modes correspond to the core and shell modes of the waveguide structure of Fig. 1. Thus, the real parts of the refractive indices $n_{r,\text{eff}}$ and $\widetilde{n}_{r,\text{eff}}$ are equal [$\Gamma>>0$ in Fig. 2(b)]. On the other hand, the imaginary parts of the refractive indices $n_{i,\text{eff}}$ and $\widetilde{n}_{i,\text{eff}}$ are associated with loss in the structure and are different ($n_{i,\text{eff}}>\widetilde{n}_{i,\text{eff}}$). The eigenvalues of this Hamiltonian are

$$n^{\pm}_{\text{eff}} = n_{r,\text{eff}} - jn^{+}_{i,\text{eff}} \pm \sqrt{\gamma^2 - (n^{-}_{i,\text{eff}})^2}, \tag{12}$$

where $n^{+}_{i,\text{eff}} = \frac{n_{i,\text{eff}}+\widetilde{n}_{i,\text{eff}}}{2}$ and $n^{-}_{i,\text{eff}} = \frac{n_{i,\text{eff}}-\widetilde{n}_{i,\text{eff}}}{2}$. As the core to total radius ratio χ increases, the coupling strength between the two propagating waveguide modes γ increases. When γ is equal to $n^{-}_{i,\text{eff}}$, an EP is formed: the two eigenvalues $n^{\pm}_{\text{eff}}$ coalesce into $n_{r,\text{eff}} - jn^{+}_{i,\text{eff}}$, and the two eigenmodes $\psi_{\pm}$ coalesce into $(1, j)^T$.

3.2. Topological properties of the exceptional points

In this subsection, to gain deeper insight into the exceptional point of the structure, we investigate the associated phenomena of level repulsion and crossing, as well as the cross conversion of the eigenvalues by encircling the EP.

It is well known that non-Hermitian quantum systems can experience a transition from level repulsion to level crossing or vice versa by the slipping of EPs over the parameter space [1–3,9]. To provide further evidence of the occurrence of an EP in the waveguide structure of Fig. 1, we calculate the real and imaginary parts of the effective indices of the propagating waveguide modes below ($n_1 = 2.865$) and above ($n_1 = 2.885$) the critical refractive index of the core layer ($n_1 = 2.875$) as a function of the core to total radius ratio χ (Fig. 4). We observe that the effective indices show level repulsion in the real parts and level crossing in the imaginary parts when the refractive index of core layer is below ($n_1 = 2.865$) the critical value of the EP. In contrast, the effective indices show level crossing in the real parts and level repulsion in the imaginary parts when the refractive index of core layer is above ($n_1 = 2.885$) the critical value of the EP.

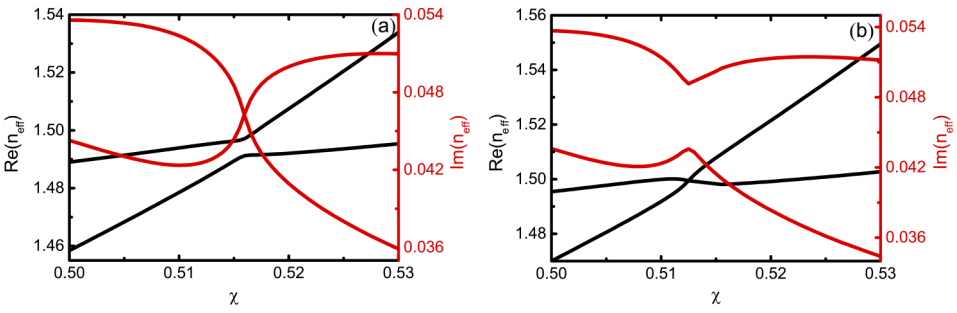

Fig. 4. (a) Real and imaginary parts of the effective indices of the propagating waveguide modes as a function of the core to total radius ratio χ for $n_1 = 2.865$. All other parameters are as in Fig. 2(a). (b) Same as in (a) except that $n_1 = 2.885$.

Another unique topological property of EPs is that, when encircling an EP in parameter space, the eigenvalues will switch their positions after a closed loop of 2π because of the square root

Optics EXPRESS

behavior of the singularity [1,4,29,30,46,53]. In our cylindrical optical waveguide structure (Fig. 1), we consider the parameter space of the refractive index of the core layer n_1 and the core to total radius ratio χ. The EP is encircled by a circular loop with a radius of ρ in the $n_1 - \chi$ plane and is located at the center of this circle ($n_1 = 2.875, \chi = 0.514$) [Fig. 5(a)]. We choose the radius ρ to be 0.01 to ensure that only the EP that we obtained by optimizing the structure is embedded inside this circle. We vary the refractive index of the core layer n_1 and the core to total radius ratio χ in the counterclockwise direction along the circular loop from the initial position A with $n_1 = 2.885, \chi = 0.514$ [Fig. 5(a)]. That is, we vary the refractive index of the core layer n_1 and the core to total radius ratio χ so that

$$n_1 = n_{1,EP} + \rho cos\theta, \chi = \chi_{EP} + \rho sin\theta, \tag{13}$$

where θ is adiabatically varied from $\theta = 0$ to $\theta = 2\pi$.

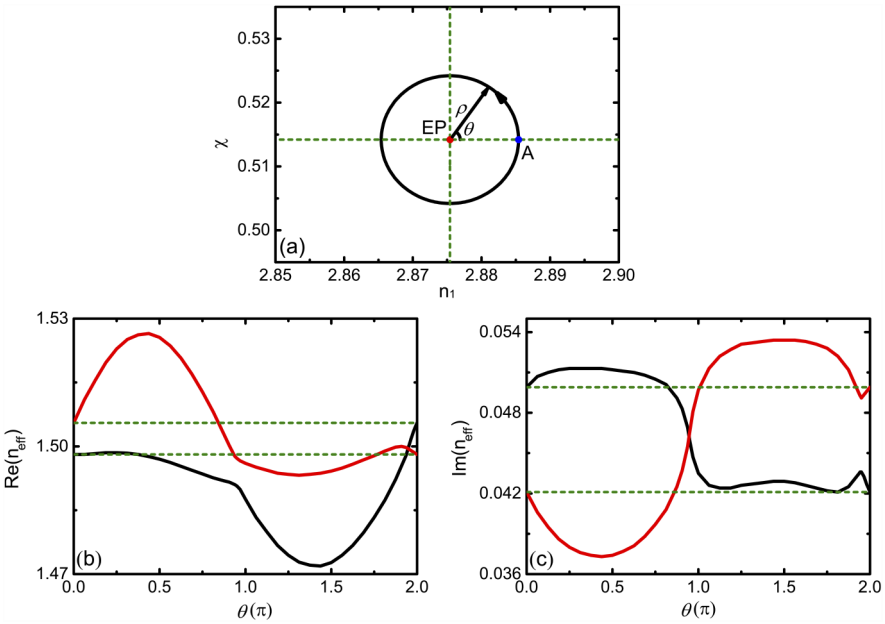

Fig. 5. (a) A circular loop in the parameter space of the refractive index of the core layer n_1 and the core to total radius ratio χ. The circle is centered at the exceptional point (red dot with $n_1 = 2.875, \chi = 0.514$), and its radius ρ is set to be 0.01. The blue dot represents the starting position of the loop (point A with $n_1 = 2.885, \chi = 0.514$). (b) and (c) The trajectories of the real and imaginary parts of the effective indices of the propagating waveguide modes for the structure of Fig. 1, as the path of the refractive index of the core layer n_1 and the core to total radius ratio χ traces the circular loop of Fig. 5(a) in the counterclockwise orientation. All other parameters are as in Fig. 2(a).

Figures 5(b) and 5(c) show the trajectories of the real and imaginary parts of the effective indices of the waveguide modes for the structure of Fig. 1, as the path of the refractive index of the core layer n_1 and the core to total radius ratio χ traces the circular loop of Fig. 5(a). We indeed observe that the two complex effective indices switch their values after one loop of 2π in the $n_1 - \chi$ plane. The cross conversion of the two eigenvalues shown in Figs. 5(b) and 5(c) further confirms the existence of the EP in our proposed two-layer cylindrical optical waveguide of Fig. 1. In contrast, if there is no EP in the closed loop, the eigenvalues will return to their initial values at the end of the loop [1]. Note that the cross conversion of the two eigenvalues implies the existence of an EP inside the loop. Taking advantage of this unique topological property of

Optics EXPRESS

EPs, the cross conversion of the two eigenvalues indicates the existence of the EP inside the loop without the need to locate the exact parameters at which the EP occurs [1]. Practical realization of the two-parameter control in our structure in order to encircle the EP, can be achieved by adiabatically varying the two parameters (refractive index of the core layer n_1 and core to total radius ratio χ) along the direction of propagation z [38]. More specifically, by setting $\theta = 2\pi z/L$ in Eq. (13), we obtain $n_1 = n_{1,EP} + \rho cos(2\pi z/L)$, $\chi = \chi_{EP} + \rho sin(2\pi z/L)$. The length parameter L should be large, so that the variation along the direction of propagation z is slow [38].

3.3. Applications of EPs in two-layer cylindrical optical waveguides

It has been demonstrated both theoretically and experimentally that EPs can enhance the sensing of nanoparticles [19,21]. More specifically, the frequency splitting at an EP is proportional to the square root of the external perturbation, whereas the response to the external perturbation at a conventional diabolic point is linear [3,19,21]. In addition, the performance of optical absorption switches is strongly dependent on the sensitivity of the imaginary part of the effective index of the waveguide mode to variations of the imaginary part of the refractive index of the active absorbing material [51]. In this subsection, we show that for our proposed two-layer cylindrical waveguide structure of Fig. 1 the sensitivity of the imaginary part of the effective index of the waveguide mode to variations of the imaginary part of the refractive index of the active absorbing material is enhanced at the EP.

When a variation of $\Delta\kappa$ is introduced into the imaginary part κ of the refractive index of the active absorbing material filling the shell layer of the waveguide (Fig. 1), the waveguide mode at the EP is perturbed and split into two modes. We define the effective index splitting Δn_{eff} as the difference between the effective indices of these two waveguide modes divided by two. Figure 6(a) shows the imaginary part of Δn_{eff} as a function of the variation $\Delta\kappa$ at the EP for $k_0 a_2 = 10$, $n_1 = 2.875$, $n_2 = 2.02 + j0.05$, $\chi = 0.514$, and $m = 6$. Similar to nanoparticle sensors in PT-symmetric optical systems based on second order EPs [21,22], we observe a square-root dependence of the effective index splitting on the variation $\Delta\kappa$. As shown in the log-log plot of Fig. 6(b), a fitting straight line (red line) with a linear slope of $\sim \frac{1}{2}$ confirms the square-root dependence of the imaginary part of the effective index splitting $\text{Im}(\Delta n_{\text{eff}})$ on the refractive index variation $\Delta\kappa$.

To characterize the sensing capability of the proposed two-layer cylindrical waveguides at EPs, we define the sensitivity $\frac{Im(\Delta n_{\text{eff}})}{\Delta\kappa}$. In addition, we consider as a reference waveguide a single-layer cylindrical waveguide with its core filled with the same active absorbing material as the one filling the shell of the waveguide in Fig. 1. We then define the sensitivity enhancement as

$$\eta = \left| \frac{Im(\Delta n_{\text{eff}})/\Delta\kappa}{Im(\Delta n_{\text{eff,single}})/\Delta\kappa} \right| = \left| \frac{Im(\Delta n_{\text{eff}})}{Im(\Delta n_{\text{eff,single}})} \right|, \tag{14}$$

where $\Delta n_{\text{eff,single}}$ is the variation in the effective index of the waveguide mode of the reference single-layer cylindrical waveguide induced by a variation $\Delta\kappa$ in the imaginary part of the refractive index of the material filling the core of the waveguide. Figure 6(c) shows the imaginary part of $\Delta n_{\text{eff,single}}$ as a function of the variation $\Delta\kappa$ for the waveguide mode of the reference single-layer cylindrical waveguide with $k_0 a_{\text{single}} = 10$ and $m = 6$. Here a_{single} is the radius of the core of the reference single-layer cylindrical waveguide. We observe that the imaginary part of $\Delta n_{\text{eff,single}}$ is linearly proportional to the perturbation $\Delta\kappa$. Figure 6(d) shows the sensitivity enhancement η [Eq. (14)] as a function of the variation in the imaginary part of the refractive index of the absorbing material $\Delta\kappa$. We observe that the sensitivity enhancement significantly increases as the refractive index variation $\Delta\kappa$ decreases, due to the square root dependence of the effective index splitting on the refractive index variation at EPs [21,22]. In other words, larger sensitivity enhancement is obtained for smaller perturbations [22].

Optics EXPRESS

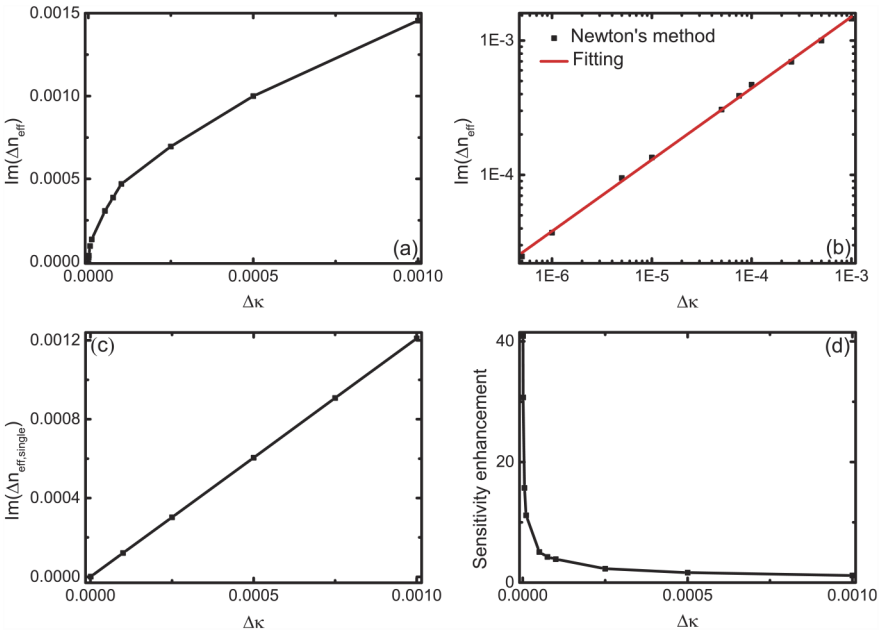

Fig. 6. (a) Imaginary part of the effective index splitting Δn_{eff} as a function of the variation $\Delta\kappa$ in the imaginary part of the refractive index of the active absorbing material filling the shell layer of the waveguide of Fig. 1 at the exceptional point. All other parameters are as in Fig. 2(a). (b) Log-log plot corresponding to (a). We show the results obtained by solving Eq. (10) numerically using Newton's method (squares), as well as a fitting straight line (red line). (c) Imaginary part of the variation $\Delta n_{\text{eff,single}}$ in the effective index of the waveguide mode of the reference single-layer cylindrical waveguide as a function of the variation $\Delta\kappa$ in the imaginary part of the refractive index of the material filling the core of the waveguide. Results are shown for $k_0 a_{\text{single}} = 10$ and $m = 6$, where a_{single} is the radius of the core of the reference single-layer cylindrical waveguide. All other parameters are as in Fig. 2(a). (d) Sensitivity enhancement η [Eq. (14)] as a function of the variation $\Delta\kappa$ in the imaginary part of the refractive index of the absorbing material. All other parameters are as in Fig. 2(a).

When a small variation of $\Delta\kappa>0$ is introduced into the imaginary part κ of the refractive index of the material filling the shell layer (Fig. 1), $n_{r,\text{eff}}$, $n^{+}_{i,\text{eff}}$, and $n^{-}_{i,\text{eff}}$ in Eq. (12) change to $n_{r,\text{eff}} + \Delta n_{r,\text{eff}}$, $n^{+}_{i,\text{eff}} + \Delta n^{+}_{i,\text{eff}}$, and $n^{-}_{i,\text{eff}} + \Delta n^{-}_{i,\text{eff}}$, where $\Delta n_{r,\text{eff}}$, $\Delta n^{+}_{i,\text{eff}}$, and $\Delta n^{-}_{i,\text{eff}}$ are also small. The eigenvalues of the Hamiltonian corresponding to the two-level model [Eq. (11)] then change to

$$n^{\pm}_{\text{eff}} \simeq n_{r,\text{eff}} + \Delta n_{r,\text{eff}} - j(n^{+}_{i,\text{eff}} + \Delta n^{+}_{i,\text{eff}}) \pm \sqrt{\gamma^2 - (n^{-}_{i,\text{eff}} + \Delta n^{-}_{i,\text{eff}})^2}. \tag{15}$$

As mentioned above, for this two-level model an EP is formed when γ is equal to $n^{-}_{i,\text{eff}}$. When the small variation of $\Delta\kappa$ is introduced, the waveguide mode at the EP is perturbed and split into two modes. The difference between the effective index of each of these waveguide modes and the effective index of the mode at the EP is given by

$$\Delta n^{\pm}_{\text{eff}} \simeq \Delta n_{r,\text{eff}} - j\Delta n^{+}_{i,\text{eff}} \pm j\sqrt{2n^{-}_{i,\text{eff}}\Delta n^{-}_{i,\text{eff}} + (\Delta n^{-}_{i,\text{eff}})^2}. \tag{16}$$

Since the variation of $\Delta\kappa$ is small, the square root term in Eq. (16) dominates, so that $\Delta n^{\pm}_{\text{eff}} \simeq \pm j\sqrt{2n^{-}_{i,\text{eff}}\Delta n^{-}_{i,\text{eff}} + (\Delta n^{-}_{i,\text{eff}})^2}$. Neglecting the second-order term $(\Delta n^{-}_{i,\text{eff}})^2$, we obtain

$$\Delta n^{\pm}_{\text{eff}} \simeq \pm j\sqrt{2n^{-}_{i,\text{eff}}\Delta n^{-}_{i,\text{eff}}} = \pm j\sqrt{(n_{i,\text{eff}} - \widetilde{n}_{i,\text{eff}})\Delta n^{-}_{i,\text{eff}}}. \tag{17}$$

Optics EXPRESS

Thus, we showed that the difference $\Delta n_{\text{eff}}^{\pm}$ between the effective index of the perturbed waveguide modes and the effective index of the mode at the EP is proportional to the square root of the difference $n_{i,\text{eff}} - \widetilde{n}_{i,\text{eff}}$ between the imaginary parts of the effective indices of the two uncoupled waveguide modes.

In Fig. 7(a) we show the evolution of the imaginary part of the effective indices n_{eff} of the two waveguide modes along the particular curve parametrized by Γ in the $\chi - n_1$ design parameter space, where either the real parts or the imaginary parts of the effective indices of the two waveguide modes coincide. We show results for different values of the imaginary part κ of the refractive index of the active material filling the shell layer (Fig. 1). We found that for $\kappa = 0.03$, $\kappa = 0.05$, and $\kappa = 0.07$ the EPs, corresponding to $\Gamma = 0$, are located at ($n_1 = 2.928, \chi = 0.505$), ($n_1 = 2.875, \chi = 0.514$), and ($n_1 = 2.829, \chi = 0.523$), respectively, in the $\chi - n_1$ plane. We observe that, as the loss in the shell layer increases, the difference between the imaginary parts of the effective indices of the two waveguide modes for Γ>0 increases. This result can indicate two points. Firstly, the variation $\Delta n_{i,\text{eff}}^{-}$ is positive when the variation of $\Delta\kappa$>0 is introduced into the shell layer. Since the factor $n_{i,\text{eff}}^{-}$ is also positive, thus the effective index splitting is mostly contributed by its imaginary component when the variation of $\Delta\kappa$ is sufficiently small [Eq. (17)]. Secondly, the imaginary part of the effective index splitting can be enhanced by increasing the loss in the shell layer based on Eq. (17). Thus, based on Eq. (17) we expect that, as the loss in the shell layer increases, the sensitivity of the structure will increase. Figure 7(b) shows the sensitivity $\frac{Im(\Delta n_{\text{eff}})}{\Delta\kappa}$ at the EP as a function of the imaginary part κ of the refractive index of the active material filling the shell layer of the waveguide (Fig. 1). In all cases, the variation in the imaginary part of the refractive index of the material filling the shell layeris $\Delta\kappa = 5 \times 10^{-4}$. As expected, we observe that the sensitivity increases as the loss in the material filling the shell layer increases.

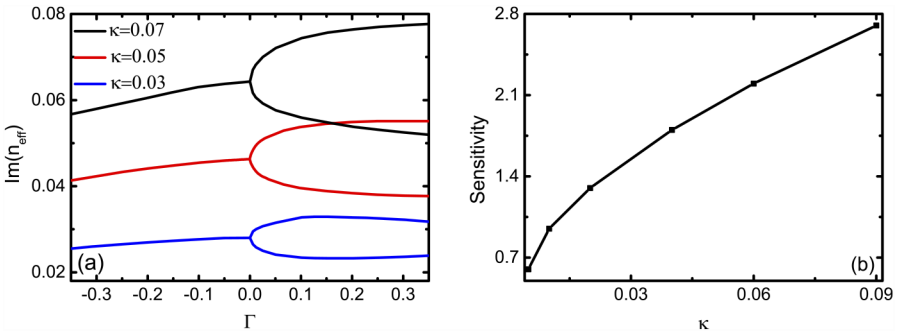

Fig. 7. (a) Imaginary parts of the effective indices n_{eff} of the two waveguide modes along the particular curve parametrized by Γ in the $\chi - n_1$ design parameter space for different values of the imaginary part κ of the refractive index of the active material filling the shell layer (Fig. 1). Results are shown for $\kappa = 0.03, 0.05$, and 0.07. All other parameters are as in Fig. 2(a). (b) Sensitivity $\frac{Im(\Delta n_{\text{eff}})}{\Delta\kappa}$ at the exceptional point as a function of the imaginary part κ of the refractive index of the active material filling the shell layer of the waveguide (Fig. 1). In all cases, the variation in the imaginary part of the refractive index of the material filling the shell layer is $\Delta\kappa = 5 \times 10^{-4}$. All other parameters are as in Fig. 2(a).

In practice, our proposed two-layer cylindrical waveguide structure can be realized using oxides such as Cu_2O for the material filling the core of the waveguide (Fig. 1). Cu_2O is lossless and has a refractive index very close to 2.875 at the wavelength of $\lambda_0 = 610$ nm [54,55]. In addition, as mentioned above, our choice for the imaginary part of the refractive index n_2 of the material filling the shell layer ($\kappa = 0.05$) is within the range of experimentally achievable values [50,51].

Optics EXPRESS

4. Conclusions

In this paper, we investigated the EP of a two-layer cylindrical waveguide structure consisting of absorbing and non-absorbing dielectrics. We used the transfer matrix method to account for the behavior of the structure. The effective indices of the propagating waveguide modes are the eigenvalues of the non-Hermitian system, and the corresponding propagating waveguide modes are the system eigenfunctions. We showed that, by tuning the core to total radius ratio and the refractive index of the core layer, the complex effective indices of two waveguide modes can coalesce so that an EP is formed. The underlying formation mechanism of the EP in our proposed two-layer cylindrical waveguide structure is associated with the interaction between two propagating modes supported by the waveguide. We found that the interaction between the two modes undergoes a transition from weak intermode interaction to strong intermode interaction, which resembles the phase transition from the PT-symmetric phase to the PT-broken phase in optical PT-symmetric systems.

We then investigated the realized EP of the structure, as well as the associated physical effects of level repulsion and crossing. We found that the level repulsion to level crossing transition in the real parts of the effective indices, and the level crossing to level repulsion transition in the imaginary parts of the effective indices occur when the refractive index of the core layer is crossing over the EP. In addition, we found that, when encircling the EP in the parametric space, the eigenvalues switch their positions after a closed loop of 2π.

Finally, we found that the sensitivity of the effective index of the waveguide mode to variations of the refractive index of the material filling the shell layer is enhanced at the EP. In addition, we showed that larger sensitivity enhancement is obtained for smaller perturbations. We also found that, as the loss in the shell layer increases, the sensitivity increases.

As final remarks, we note that the proposed two-layer cylindrical structures can be fabricated by combining chemical vapor deposition and atomic layer deposition [56–58]. Even though here we investigated EPs for azimuthal mode number $m = 6$, EPs exist for other azimuthal mode numbers as well. As an example, an EP exists for $n_1 = 2.450$, $\chi = 0.462$ when $m = 7$. Selective excitation of the individual modes of a multimode waveguide can be realized using fiber Binary phase spatial light modulators [59]. In addition, here we investigated the sensitivity of the effective index of the waveguide mode to variations of the refractive index of the material filling the shell layer, and showed that the sensitivity is enhanced at the EP. Similarly, we expect that the sensitivity to variations of the refractive index of the material surrounding the two-layer cylindrical structure will also be enhanced at the EP. Thus, our results could potentially contribute to the development of a new generation of chip-scale exceptional-point-enhanced optical waveguide devices for modulation, switching, and sensing.

Funding

National Natural Science Foundation of China (61605252); Natural Science Foundation of Hunan Province (2017JJ3375); National Science Foundation (1254934).

Disclosures

The authors declare that there are no conflicts of interest related to this article.

References

1. N. Moiseyev, *Non-Hermitian Quantum Mechanics* (Cambridge University, 2011).
2. W. Heiss, "Exceptional points of non-Hermitian operators," J. Phys. A: Math. Gen. **37**(6), 2455–2464 (2004).
3. W. Heiss, "Repulsion of resonance states and exceptional points," Phys. Rev. E **61**(1), 929–932 (2000).
4. C. Dembowski, H. Graf, H. Harney, A. Heine, W. Heiss, H. Rehfeld, and A. Richter, "Experimental observation of the topological structure of exceptional points," Phys. Rev. Lett. **86**(5), 787–790 (2001).

Optics EXPRESS

5. S. Ozdemir, S. Rotter, F. Nori, and L. Yang, "Parity-time symmetry and exceptional points in photonics," Nat. Mater. **18**(8), 783–798 (2019).
6. Y. Shin, H. Kwak, S. Moon, S. Lee, J. Yang, and K. An, "Observation of an exceptional point in a two-dimensional ultrasonic cavity of concentric circular shells," Sci. Rep. **6**(1), 38826 (2016).
7. O. Kirillov, "Exceptional and diabolical points in stability questions," Fortschr. Phys. **61**(2-3), 205–224 (2013).
8. T. Stehmann, W. Heiss, and F. Scholtz, "Observation of exceptional points in electronic circuits," J. Phys. A: Math. Gen. **37**(31), 7813–7819 (2004).
9. W. Heiss, "The physics of exceptional points," J. Phys. A: Math. Theor. **45**(44), 444016 (2012).
10. Z. Musslimani, K. Makris, R. Ganainy, and D. Christodoulides, "Optical solitons in *PT*-periodic potentials," Phys. Rev. Lett. **100**(3), 030402 (2008).
11. C. Ruter, K. Makris, R. El-Ganainy, D. Christodoulides, M. Segev, and D. Kip, "Observation of parity-time symmetry in optics," Nat. Phys. **6**(3), 192–195 (2010).
12. L. Chang, X. Jiang, S. Hua, C. Yang, J. Wen, L. Jiang, G. Li, G. Wang, and M. Xiao, "Parity-time symmetry and variable optical isolation in active-passive-coupled microresonators," Nat. Photonics **8**(7), 524–529 (2014).
13. Z. Lin, H. Ramezani, T. Eichelkraut, T. Kottos, H. Cao, and D. Christodoulides, "Unidirectional invisibility induced by *PT*-symmetric periodic structures," Phys. Rev. Lett. **106**(21), 213901 (2011).
14. L. Feng, Y. Xu, W. Fegadolli, M. Lu, J. Oliveira, V. Almeida, Y. Chen, and A. Scherer, "Experimental demonstration of a unidirectional reflectionless parity-time metamaterial at optical frequencies," Nat. Mater. **12**(2), 108–113 (2013).
15. Y. Huang, G. Veronis, and C. Min, "Unidirectional reflectionless propagation in plasmonic waveguide-cavity systems at exceptional points," Opt. Express **23**(23), 29882–29895 (2015).
16. Y. Sun, W. Tan, H. Li, J. Li, and H. Chen, "Experimental demonstration of a coherent perfect absorber with *PT* phase transition," Phys. Rev. Lett. **112**(14), 143903 (2014).
17. Y. Chong, L. Ge, and A. Stone, "*PT*-symmetry breaking and laser-absorber modes in optical scattering systems," Phys. Rev. Lett. **106**(9), 093902 (2011).
18. Y. Huang, C. Min, and G. Veronis, "Broadband near total light absorption in non-*PT*-symmetric waveguide-cavity systems," Opt. Express **24**(19), 22219–22231 (2016).
19. J. Wiersig, "Enhancing the sensitivity of frequency and energy splitting detection by using exceptional points: application to microcavity sensors for single-particle detection," Phys. Rev. Lett. **112**(20), 203901 (2014).
20. H. Hodaei, A. Hassan, S. Wittek, H. Gracia, R. Ganainy, D. Christodoulides, and M. Khajavikhan, "Enhanced sensitivity at higher-order exceptional points," Nature **548**(7666), 187–191 (2017).
21. W. Chen, S. Ozdemir, G. Zhao, J. Wiersig, and L. Yang, "Exceptional points enhance sensing in an optical microcavity," Nature **548**(7666), 192–196 (2017).
22. W. Chen, J. Zhang, B. Peng, S. Ozdemir, X. Fan, and L. Yang, "Parity-time-symmetric whispering-gallery mode nanoparticle sensor," Photonics Res. **6**(5), A23–A30 (2018).
23. B. Peng, S. Ozdemir, M. Liertzer, W. Chen, J. Kramer, H. Yilmaz, J. Wiersig, S. Rotter, and L. Yang, "Chiral modes and directional lasing at exceptional points," Proc. Natl. Acad. Sci. U. S. A. **113**(25), 6845–6850 (2016).
24. S. Longhi and L. Feng, "Unidirectional lasing in semiconductor microring lasers at an exceptional point," Photonics Res. **5**(6), B1–B6 (2017).
25. S. Yu, X. Piao, and N. Park, "Neuromorphic functions of light in parity-time-symmetric systems," Sci. Adv. **6**, 1900771 (2019).
26. T. Goldzak, A. Mailybaev, and N. Moiseyev, "Light stops at exceptional points," Phys. Rev. Lett. **120**(1), 013901 (2018).
27. S. Gangaraj and F. Monticone, "Topological waveguiding near an exceptional point: defect-immune, slow-light, and loss-immune propagation," Phys. Rev. Lett. **121**(9), 093901 (2018).
28. S. Wang, B. Hou, W. Lu, Y. Chen, Z. Zhang, and C. Chan, "Arbitrary order exceptional point induced by photonic spin-orbit interaction in coupled resonators," Nat. Commun. **10**(1), 832 (2019).
29. J. Doppler, A. Mailybaev, J. Bohm, U. Kuhl, A. Girschik, F. Libisch, T. Milburn, P Rabl, N. Moiseyev, and S. Rotter, "Dynamically encircling an exceptional point for asymmetric mode switching," Nature **537**(7618), 76–79 (2016).
30. B. Zhen, C. Hsu, Y Igarashi, L. Lu, I. Kaminer, A. Pick, S. Chua, J. Joannopoulos, and M. Soljacic, "Spawning rings of exceptional points out of Dirac cones," Nature **525**(7569), 354–358 (2015).
31. W. Wang, L. Wang, R. Xue, H. Chen, R. Guo, Y. Liu, and J. Chen, "Unidirectional excitation of radiative-loss-free surface plasmon polaritons in *PT*-symmetric systems," Phys. Rev. Lett. **119**(7), 077401 (2017).
32. H. Zhao, W. Fegadolli, J. Yu, Z. Zhang, L. Ge, A. Scherer, and L. Feng, "Metawaveguide for asymmetric interferometric light-light switching," Phys. Rev. Lett. **117**(19), 193901 (2016).
33. Z. Lin, A. Pick, M. Loncar, and A. Rodriguez, "Enhanced spontaneous emission at third-order Dirac exceptional points in inverse-designed photonic crystals," Phys. Rev. Lett. **117**(10), 107402 (2016).
34. Q. Xie, S. Rong, and X. Liu, "Exceptional points in a time-periodic parity-time-symmetric Rabi model," Phys. Rev. A **98**(5), 052122 (2018).
35. S. Yu, H. Park, X. Piao, B. Min, and N. Park, "Low-dimensional optical chirality in complex potentials," Optica **3**(9), 1025–1032 (2016).
36. S. Klaiman, U. Gunther, and N. Moiseyev, "Visualization of branch points in *PT*-symmetric waveguides," Phys. Rev. Lett. **101**(8), 080402 (2008).

Optics EXPRESS

37. H. Alaeian, B. Baum, V. Jankovic, M. Lawrence, and J. Dionne, "Towards nanoscale multiplexing with parity-time-symmetric plasmonic coaxial waveguides," Phys. Rev. B **93**(20), 205439 (2016).
38. S. Ke, B. Wang, C. Qin, H. Long, K. Wang, and P. Lu, "Exceptional points and asymmetric mode switching in plasmonic waveguides," J. Lightwave Technol. **34**(22), 5258–5262 (2016).
39. S. Ghosh and Y. Chong, "Exceptional points and asymmetric mode conversion in quasi-guided dual-mode optical waveguides," Sci. Rep. **6**(1), 19837 (2016).
40. X. Yin and X. Zhang, "Unidirectional light propagation at exceptional points," Nat. Mater. **12**(3), 175–177 (2013).
41. Y. Huang, Y. Shen, C. Min, S. Fan, and G. Veronis, "Unidirectional reflectionless light propagation at exceptional points," Nanophotonics **6**(5), 977–996 (2017).
42. M. Skorobogatiy, *Nanostructured and Subwavelength Waveguides* (Wiley, 2012).
43. Z. Yang, R. Jiang, X. Zhuo, Y. Xie, J. Wang, and H. Lin, "Dielectric nanoresonators for light manipulation," Phys. Rep. **701**, 1–50 (2017).
44. Y. Huang, Z. Zhen, Y. Shen, C. Min, and G. Veronis, "Optimization of photonic nanojets generated by multilayer microcylinders with a genetic algorithm," Opt. Express **27**(2), 1310–1325 (2019).
45. Z. Zhen, Y. Huang, Y. Feng, Y. Shen, and Z. Li, "An ultranarrow photonic nanojet formed by an engineered two-layer microcylinder of high refractive-index materials," Opt. Express **27**(6), 9178–9188 (2019).
46. Y. Huang, Y. Shen, C. Min, and G. Veronis, "Switching of the direction of reflectionless light propagation at exceptional points in non-*PT*-symmetric structures using phase-change materials," Opt. Express **25**(22), 27283–27297 (2017).
47. C. Kelley, *Solving Nonlinear Equations with Newton's Method* (Society for Industrial and Applied Mathematics, 2003).
48. R. Reddy, K. Gopal, K. Narasimhulu, L. Reddy, K. Kumar, G. Balakrishnaiah, and M. Kumar, "Interrelationship between structural, optical, electronic and elastic properties of materials," J. Alloys Compd. **473**(1-2), 28–35 (2009).
49. D. Pacifici, H. Lezec, and H. Atwater, "All-optical modulation by plasmonic excitation of CdSe quantum dots," Nat. Photonics **1**(7), 402–406 (2007).
50. D. Pacifici, H. Lezec, L. Sweatlock, C. Ruiter, V. Ferry, and H. Atwater, "All-optical plasmonic modulators and interconnects," in *Plasmonic nanoguides and circuits*, S. I. Bozhevolnyi, ed. (World Scientific, 2009).
51. C. Min and G. Veronis, "Absorption switches in metal-dielectric-metal plasmonic waveguides," Opt. Express **17**(13), 10757–10766 (2009).
52. J. Kullig, C. Yi, M. Hentschel, and J. Wiersig, "Exceptional points of third-order in a layered optical microdisk cavity," New J. Phys. **20**(8), 083016 (2018).
53. Q. Liu, B. Wang, S. Ke, H. Long, K. Wang, and P. Lu, "Exceptional points in Fano-resonant graphene metamaterials," Opt. Express **25**(7), 7203–7212 (2017).
54. D. Tahir and S. Tougaard, "Electronic and optical properties of Cu, CuO and Cu_2O studied by electron spectroscopy," J. Phys.: Condens. Matter **24**(17), 175002 (2012).
55. A. Rakhshani and J. Varghese, "Optical absorption coefficient and thickness measurement of electrodeposited films of Cu_2O," Phys. Status Solidi (A) **101**(2), 479–486 (1987).
56. L. Zhang, R. Tu, and H. Dai, "Parallel core-shell metal-dielectric-semiconductor germanium nanowires for high-current surround-gate field-effect transistors," Nano Lett. **6**(12), 2785–2789 (2006).
57. J. Sun, R. Deacon, R. Wang, J. Yao, C. Lieber, and K. Ishibashi, "Helical hole state in multiple conduction modes in Ge/Si core/shell nanowire," Nano Lett. **18**(10), 6144–6149 (2018).
58. X. Yuan, L. Li, Z. Li, F. Wang, N. Wang, L. Fu, J. He, H. Tan, and C. Ja, "Unexpected benefits of stacking faults on the electronic structure and optical emission in wurtzite GaAs/GaInP core/shell nanowires," Nanoscale **11**(18), 9207–9215 (2019).
59. J. Carpenter and T. Wilkinson, "Characterization of multimode fiber by selective mode excitation," J. Lightwave Technol. **30**(10), 1386–1392 (2012).